Title
STRUCTURAL OBSERVATIONS IN A METASTABLE AUSTENITIC STEEL.

Author
Hall, James A.

Publication Date
1968-06-01

UCRL-18282

Cy. 2

University of California

Ernest O. Lawrence Radiation Laboratory

STRUCTURAL OBSERVATIONS IN A METASTABLE AUSTENITIC STEEL

James A. Hall

(M. S. Thesis)

June 1968

Berkeley, California

UCRL-18282
Cy. 2

DISCLAIMER

UCRL-18282

UNIVERSITY OF CALIFORNIA

Lawrence Radiation Laboratory
Berkeley, California
AEC Contract No. W-7405-Eng-48

STRUCTURAL OBSERVATIONS IN A METASTABLE AUSTENITIC STEEL

James A. Hall

(M.S. Thesis)

June 1968

TABLE OF CONTENTS

STRUCTURAL OBSERVATIONS IN A METASTABLE AUSTENITIC STEEL

James A. Hall

Inorganic Materials Research Division, Lawrence Radiation Laboratory,
Department of Mineral Technology, College of Engineering,
University of California, Berkeley, California

ABSTRACT

A metastable austenitic steel of composition Fe 22.6Ni 4.02Mo .28C shows very favorable response to a thermomechanical treatment consisting of deformation at an elevated temperature. In room temperature tensile tests, this processed austenitic steel shows large increases in yield and tensile strengths (300% and 67% respectively) while still exhibiting uniform elongations of 40% or more. These favorable properties arise as a result of a strain induced martensite transformation.

This thermomechanical treatment (called TRIP) is described and the room temperature tensile properties are given. Some structural observations with regard to microstructure and the strain induced martensitic transformation are made with some analogies to the ausforming process being described. A mechanism for the enhanced ductility is discussed in light of the evidence of this investigation.

I. INTRODUCTION

The three commonly measured engineering properties are yield strength, tensile strength, and ductility. Strength in steels has been developed in recent years to very high levels. When the high strengths are obtained by conventional heat treatments, there is a reciprocal relationship between strength and ductility, when ductility is taken to be a measure of total elongation in a tensile test.

Ductility is important from an engineering point of view since adequate ductility allows the metal to redistribute localized stresses. If the metal is capable of sustaining little or no strain prior to fracture, then it is described as brittle. Uniform elongation as a measure of ductility, rather than reduction of area, is important in many metal forming operations such as deep drawing.

Much work has been expended by many investigators in attempts to discover methods of increasing strength and ductility concurrently. A recent paper by Zackay et al.[1] discussed a new class of metastable austenitic steels which exhibit greatly enhanced ductility along with high strength. They have termed these steels TRIP (TRansformation Induced Plasticity) because the ductility is derived from the strain induced martensitic transformation. The processing of these steels involves a thermo-mechanical treatment similar to that in the ausforming process, the difference being that TRIP steels are not converted to martensite but are used in the metastable austenitic state.

It is the purpose of this investigation to study the structure of one of these TRIP steels in an attempt to gain a better understanding

of the TRIP phenomenon. For this purpose, a TRIP steel of simple composition is chosen (Fe 22.6Ni 4.02 Mo .28C).

Because the processing of TRIP steels is quite similar to the thermomechanical treatment in the ausforming process, the current state of knowledge of this latter process will be discussed in some detail as an introduction to TRIP steels.

The ausforming process was first described some years ago by Lips and Van Zuilen[2] and followed by many others.[3-7] It primarily involves the mechanical deformation of a metastable austenite at an elevated temperature below the recrystallization temperature followed by quenching to obtain martensite.

Ausforming, in many steels, sharply increases the strength of the subsequently formed martensite while retaining adequate ductility. It has been pointed out by many authors, including Tamura,[8] that the martensite formed athermally from deformed austenite, in ausformed steels, inherits many of the defects introduced during deformation.

Cohen and Taranto[9] point out that the high density of entangled dislocations carried over into the ausformed martensite from the strain hardened austenite is not sufficient to account for the strengthening that is commonly observed. They show that even though these imperfections are undoubtedly responsible for strengthening the strain-hardened austenite, they do not contribute equally to the strengthening of the martensite formed from this austenite. In a Fe 31.9Ni .017C alloy they report that with a 75% reduction of the austenite by rolling, its yield strength increases by 45,000 psi, while that of the martensite formed from such austenite increases by only 22,000 psi. Yet, the regular martensite

is quite susceptible to strengthening by strain hardening, it increases in yield strength by 54,000 psi when reduced 75% in rolling.

Greater increases in strength are observed in ausformed steels which contain carbon and a carbide forming alloying element. Thomas et al.,[10] Johari et al.,[11] and Gerberich et al.[12] conclude that carbon is an essential contributor to the strength of the ausformed steels by providing the means (together with an alloy carbide former), of forming precipitates during deformation of the metastable austenite. By utilizing the dark field technique in transmission electron microscopy, they confirmed the existance of small precipitates in the ausformed austenite in a series of alloys including one of very similar composition (Fe 25Ni 4.5Mo .28C) to the alloy used in this present study. The role that these very small precipitates play in the ausformed steels is as follows: The strength of the martensite is due mostly to the total dislocation density. Part of these dislocations arise from the transformation strains and many of them are inherited from the ausformed austenite. However, the important role of the precipitates is to cause dislocation multiplication at the particles. In other words, the precipitate particles in the ausformed austenite are indirectly responsible for the increase in strength. The ductility of the ausformed steels is retained because of the high density of mobile dislocations in the ausformed martensite.

In order to obtain large amounts of elongation at any strength level, it is necessary to prevent the onset of tensile instability. This is defined as the maximum in the load-elongation curve where the work hardening will not keep up with the reduction in area. At this point, a weaker area begins to elongate slightly more than the rest. Then, since the area is now reduced, further deformation will occur at this

weak point and necking will commence until failure. After Tegart[13], the criteria for necking will be discussed.

Since necking commences at maximum load, the condition of instability is defined as the point where $dP = 0$. Since the load is equal to the stress times the area, $P = \sigma A$, then

$$dP = \sigma dA + A d\sigma = 0$$

$$\text{ie, } -\frac{dA}{A} = \frac{d\sigma}{\sigma} \tag{1}$$

For a ductile metal, necking occurs at strains beyond yielding where the constant volume, V, condition holds:

$$dV = A d\ell + \ell dA = 0$$

$$\text{ie, } -\frac{dA}{A} = \frac{d\ell}{\ell} = d\epsilon \tag{2}$$

Substituting for dA/A from Eq. (1) gives

$$\frac{d\sigma}{\sigma} = d\epsilon$$

$$\text{ie, } \frac{d\sigma}{d\epsilon} = \sigma \tag{3}$$

Thus necking will occur in uniaxial tension at a strain at which the slope of the true stress-true strain curve equals the true stress at that strain. When expressing Eq. (3) in terms of conventional strain, we get

$$\frac{d\sigma}{de} = \frac{\sigma}{1+e} \tag{4}$$

where e is the conventional strain $(\ell - \ell_0)/\ell_0$.

The necking condition can also be expressed in terms of the strain hardening exponent "n" when the stress-strain curve follows the relationship $\sigma = k\epsilon^n$. The strain hardening exponent "n" is then

$$n = \frac{d \log_e \sigma}{d \log_e \epsilon} = \frac{\epsilon}{\sigma} \frac{d\sigma}{d\epsilon}$$

and thus from Eq. (3) we get:

$$\epsilon_{necking} = n \qquad (5)$$

That is, necking occurs when the true strain equals the strain-hardening exponent. If the $\log_e \sigma - \log_e \epsilon$ plot derived from a particular stress-strain curve is a straight line, then the power law is a satisfactory representation of the stress-strain behavior of that material.

The above discussion points out that the strain is equal to the work hardening exponent when necking begins, or in other words, a higher work hardening exponent will promote higher uniform elongations in the tensile test.

The normally used methods of strengthening steels (quench and tempering) generally tend to reduce the work hardening exponent over that in the unhardened state and the work hardening rate $d\sigma/d\epsilon$ remains relatively insensitive to the strength. Hence, in these steels plastic instability begins at lower strains because the rate of work hardening produced by dislocation interactions is insufficient to compensate for the increase in stress in the necked region.

It is evident from Eqs. (3) and (5) that when higher strengths are obtained, there must also be a higher work hardening exponent in order to allow high uniform elongations without necking. When higher strengths are obtained by conventional heat treatments, the work hardening rates are decreased. This may be understood when considering the mechanism of raising the yield strength being that of immobilization of the dislocations.

However, these mechanisms are not effective, at high stresses, in providing a high work hardening rate. In order to realize the benefits of high yield strength and high work hardening rate, the mechanism providing the higher yield strength must be present prior to testing while the predominant mechanism of increasing the work hardening rate must be introduced during testing. In other words the dislocations must be immobilized after yielding not before it, in order to obtain high work hardening.

Several authors have recognized that certain phase transformations concurrent with straining will promote high work hardening rates and the resultant high elongation. Hiltz[14] pointed out that in certain titanium alloys there occurs a strain induced martensitic transformation which enhances the ductility due to the high work hardening rate. Bressanelli and Moskowitz[15] found similar behavior in metastable austenitic stainless steels.

Until recently these investigations and others have been limited to relatively low strength materials. Zackay et al. used just this mechanism to promote elongation in high strength metastable austenitic steels. They report six compositions which exhibit a strain induced martensitic transformation in the austenite when tested in tension at room temperature. The compositions of these steels are listed in Table I.

The TRIP steels are thermomechanically treated by deformation in the temperature range of 200°C to 500°C, followed by quenching to room temperature. They are austenitic at this stage. When testing in tension at room temperature, elongations approaching 70% are obtained while yield strengths up to 300,000 psi are formed.

Table I. Chemical composition of TRIP steels composition wt.%

	Cr	Ni	Mo	Mn	Si	C
1	8.89	8.31	3.80	2.02	1.92	0.31
2	8.88	7.60	4.04	2.08	1.96	0.25
3	8.80	7.80	4.00	0.92	1.90	0.25
4	-	24.4	4.10	-	-	0.25
5	-	22.0	4.00	1.48	-	0.23
6	-	20.97	3.57	1.48	-	0.24

Zackay et al.,[1] in their paper, attribute the high yield strengths to the work hardened state of the austenite. The resistance to necking is a result of the introduction of the second phase, martensite, during the room temperature tensile test. This strain induced martensite provides barriers to dislocation motion stronger than dislocation tangles thereby causing an increase in work hardening. The resulting higher work hardening exponent raises the stress at which necking occurs (Eq. 5) thereby allowing greater amounts of uniform elongation.

This thesis is concerned with a study of the mechanisms of the TRIP phenomenon proposed by Zackay et al.[1]

II. EXPERIMENTAL PROCEDURE

The alloy under investigation was prepared and studies were made on the effect of the amount of thermomechanical deformation on the room temperature tensile properties. The effect of the tensile specimen orientation with respect to the rolling direction was studied.

Electron microscopy, optical microscopy and other techniques were used in conjunction with analysis of the room temperature stress-strain curves to postulate the mechanisms of the TRIP phenomenon and why such high elongations are obtained concurrently with high strength.

A. Material Preparation[1]

The alloy was prepared by vacuum induction melting and poured into a copper mold. The resulting 20 lb. ingots were forged at 1100°C to bars 3 in. × 6 in. Preliminary forming was done at 900°C by rolling. This was followed by an austenitizing treatment of one hour at 1100°C and water quenching. The thermomechanical treatment was carried out by heating in an electric oven to 500 C and then rolling the sheet in increments of 10% reduction in thickness. Each pass through the rolls was followed by reheating to 500°C. After the last pass the strip was quenched in water. This treatment will be referred to hereafter as PDA (Prior Deformation of Austenite).

B. Mechanical Tests

The tensile specimens were polished with the removal of .010 in. from each surface in order to eliminate the possible effects of surface decarburization or roll chill. The same procedure was used for the study of surface topology. The tensile specimens were flat with a gage section

.060 in.×.380 in.×1.38 in. long. Samples were cut at 0°, 45° and 90° with respect to the PDA rolling direction.

An Instron 5000 kilogram tensile machine was used at a crosshead speed of 0.1 cm/min. Trial runs with crosshead speeds greater than 1.0 cm/min caused severe reduction in ultimate tensile strength due to heat of the martensitic transformation which stabilized the austenite. Strain measurement was performed utilizing a one-inch extensometer calibrated to 60% extension with the output fed into the chart drive system of the Instron control console.

C. Optical Microscopy

The specimens were electropolished in a saturated solution of chromic oxide in phosphoric acid and electroetched in the same solution after it had been observed that martensite was being nucleated as a result of mechanical polishing. If this was not observed, conventional metallographic polishing techniques were used. When necessary, a supplemental etch consisting of 5 grams cupric chloride in 100 cc each of water, hydrochloric acid and methyl alcohol was used.

D. Electron Microscopy

Thin foils were prepared by light mechanical grinding from .060 in. to about .040 in. then chemically polished to about .005 in. in a 50% solution of H_2O_2 in phosphoric acid. Final thinning was accomplished by electropolishing using the window technique in the same polishing solution used for optical metallographic polishing. A current density of about 10 amperes per square inch was used.

A Siemens Elmiskop IA electron microscopy operated at 100 kV was used for transmission microscopy.

E. Differential Thermal Analysis

The differential thermal analysis tests were made by using the

specimen and a nickel standard. Both were 1 cm × 1 cm × .030 in. and spot welded to iron-constantan thermocouples. Heating was done in an argon atmosphere, recording simultaneously the temperature of the specimen and the difference between the standard and specimen temperatures. When the reversion of the martensite to austenite occurred, a sudden change in the differential temperature curve was recorded. This was taken to be the A_s (austenite start) temperature.

F. Electron Microprobe Analysis

A step trace measuring Mo L_α radiation was made across the bands in microstructure. The L_α line was used rather than K_α or K_β because the wavelengths of these are so small that the analyzing detector was unable to be positioned at low enough angle for efficient detection. Quantitative measurements were not possible since the minimum electron beam spot size was larger than the average precipitate size. Therefore, only the Mo L_α intensity in terms of counts per 10 sec period were measured and plotted.

G. Distribution of Martensite in Tensile Samples

Prior to testing, the surface layer was removed by electropolishing to a depth of .010 in. (to remove any effect of decarburization or surface roll chill) and then polished. After a tensile extension of 15%, successive material removal from the surface was done by electropolishing. At each stage several micrographs were taken at a magnification of 400×.

To measure the volume percent martensite at each level, the grid intercept-point count method was used.[16] At least six 4×5 micrographs, each divided into 2000 grid intersections, were used to determine each datum point.

H. Magnetic Measurements

The failed tensile specimens were cut 3/8 in. back from each side of the fracture and then both pieces were measured for magnetic saturization which had previously been correlated with the volume percent martensite.[17] The values of volume percent martensite were measured in failed specimens as functions of amount of prior deformation and orientation. The correction for alloy content was made according to the data of Kittel.[18]

III. EXPERIMENTAL RESULTS

A. Mechanical Tests

The tests made for room temperature property studies of the PDA are summarized in the stress-strain curves of Figs. 1 through 5. These stress-strain curves typify the effects of amount of thermo-mechanical deformation and orientation with respect to the PDA rolling direction. These specimens were all austenitic prior to testing, and after the test the gage sections were strongly magnetic, indicating that a martensitic reaction occurred during the room temperature straining. No tests were run to determine just exactly when the martensite first appeared. However, when a Luders strain occurred, the martensite first appeared at the first yield or load drop. The occurrance of the first martensite was less definitive when there was no Luders strain.

1. Effect of amount of deformation during thermomechanical treatment.

Increased amounts of PDA resulted in the expected higher yield and tensile strengths. The results are summaried in Fig. 6. The total elongations to failure decreased to a point then seemed to increase with greater amounts of PDA as shown in Fig. 10. The work hardening exponent "n" first increased with amount of PDA, then decreased. The work hardening rate, $d\sigma/d\epsilon$, at particular strains, varied with amount of PDA in much the same manner as the value of "n". Figures 11 through 14 summarize these results. The assumption of the $\sigma = k\epsilon^n$ relationship is well borne out for that part of the stress strain curve between the Luders strain and the maximum load as seen by the straight line plots of $\log_e \sigma - \log_e \epsilon$ shown in Figs. 15a to 15j.

With more than 10% PDA, the material exhibited a Luders strain during tensile testing as shown in the stress-strain curves. Figure 16 shows one tensile specimen after incomplete passage of one such Luders band. The material inside the Luders band strongly attracted a hand magnet while that outside did not, demonstrating that the Luders band front separates the transformed from the untransformed regions.

As will be discussed later, the total amount of martensite formed at 15% elongation in specimens of the same orientation varied little with amount of prior deformation. The 15% elongation was approximately the amount of Luders strain.

2. Effect of orientation

The yield strengths showed no significant variation with orientation with respect to the rolling direction of the PDA. Figure 6 summarizes this effect.

The greatest variations with respect to PDA rolling direction were seen in tensile strength, work hardening exponent and total elongation. Both the tensile strength and work hardening exponent showed significant maxima in the specimens cut at 45° to the PDA rolling direction while the total elongation shows a minimum for the same specimen. The specimens cut parallel to the rolling direction give results similar to those from the specimens cut at 90° to the PDA rolling direction. Figures 6, 7, and 9 summarize these results.

The work hardening rate, $d\sigma/d\varepsilon$, at particular strains, varied with amount of PDA in much the same manner as the values of "n", the higher values were in specimens cut at 45° to the PDA rolling direction. It

wasthese 45° tensile samples which showed the greater amounts of martensite at fracture. Figures 12 through 14 show the plots of strain hardening rate vs deformation for strains of .15, .20, and .25.

3. Detail in the stress-strain curves.

All of the stress-strain curves had superimposed upon them numerous serrations consisting of rapid load drops followed by short areas of quite high work hardening. These serrations were not detected during Luders strain nor were they detected below about 9% ϵ on the stress-strain curves of the material which showed no Luders strain. The magnitude of the load drops increased as the stress increased and became a maximum after the onset of necking.

4. Effect of transforming the martensite prior to testing.

A specimen with 10% PDA was then transformed by immersing in liquid nitrogen and showed an increase in yield strength from 87 to 186 ksi and tensile strength from 126,000 to 200,000 psi over the material with identical PDA but not quenched in liquid nitrogen. The total elongation decreased from 54% to 11.5%.

B. Microscopy

1. After thermomechanical treatment, prior to room temperature testing.

All the PDA material, when examined in cross section exhibited a "banded" microstructure: the "banding" becoming more severe with increased amounts of PDA. Figure 17 is one such cross section showing the typically banded microstructure. An electron microprobe step-scan trace across a band gave high peaks in the measured molybdenum L_α radiation indicating precipitation of a molybdenum compound. The trace is shown

in Fig. 18. Transmission electron diffraction in a thin foil carefully prepared to retain the precipitates reveals them to be Mo_2C. An indexed electron diffraction pattern obtained is shown in Fig. 20c while Figs. 20a and 20b show bright and dark field micrographs of the areas. Two precipitates were included in the selected area giving the two HCP diffraction patterns superimposed on the pattern for the FCC matrix. One diffraction spot from each HCP pattern was included in the aperture when taking the dark field micrograph.

The undeformed material, although showing no precipitation, does indicate the presence of chemical segregation indicated by the fact that this material, when quenched to just below its Ms temperature, formed martensite in bands. A typical example of this is Fig. 21.

Transmission microscopy shows an increase in dislocation density with increasing amounts of PDA. There was a "cellular" type substructure in the 10% PDA material. The 20% and 30% PDA material showed less cellular dislocation arrangement with more nearly uniform tangles. Figures 22a, b, and c are typically observed transmission micrographs for 0, 10, and 30% deformed material.

2. <u>After room temperature tensile tests</u>

The general morphology of the strain induced martensite does not vary much in appearance with the amount of prior deformation. Figures 23b and 23c are representative of the morphology of the strain induced martensite found after 15% room temperature elongation in tension on 10% and 20% PDA material. The same morphology of strain induced martensite is observed in the material receiving 30% prior deformation. Typically

observed morphology of the strain induced martensite in the material having had no prior deformation is somewhat different, as seen in Fig. 23a.

In some areas of the strained tensile samples, the martensite appears at an angle to the tensile axis near 54.7°, which is the angle of the necking line in flat tensile specimens at the point of tensile instability.[19] These platelets occur in parallel arrays, typified by Fig. 24.

In transmission electron microscopy, the strain induced martensite appears to be free of internal twinning but contains a very dense dislocation network. Examples of this are seen in Figs. 25a and 25b. The electron diffraction pattern and micrographs give no evidence of twinning or precipitation, however under prolonged beam heating some precipitates were observed indicating that nuclei or very small precipitates had been present. It must be emphasized that in a highly dislocated microstructure the point resolution is only about 50Å; therefore precipitates this size or smaller would not be resolved. Also, since the low index planes of Mo_2C have approximately the same "d" spacings as the martensite, no evidence would be obtained in the selected area diffraction pattern due to superposition of the diffraction spots.

When a tensile test was stopped prior to complete passage of the Luders band on a polished specimen, it was found that the material inside the Luders band was highly ferromagnetic as indicated by attraction to a strong hand magnet. That area outside the Luders band remained austenitic as denoted by the same test. Considerable plastic deformation occurs outside the Luders band as shown by the presence of slip lines on the

prepolished surface. Figure 16 shows this. Figure 16a shows the specimen at the stage when the tensile test was terminated. Inside the Luders band these slip traces persist but become kinked due to the surface upheavals characteristic of the martensitic transformation. It is seen in Fig. 16c, compared to Fig. 16b, that considerable change takes place as the Luders front passes along the specimen.

In the material receiving no PDA, when strained to 5% elongation at room temperature, the resulting surface upheavals contain sharp needle like upheavals while those appearing in the Luders band show larger upheavals. Figure 26 shows this prepolished surface of the material with no PDA after room temperature straining.

In this latter specimen, removal of just .003 in. from the surface removed nearly completely all evidence of martensite. This indicates that the strain induced martensite first occurs at the surface. Tensile samples of the material receiving 10, 20, and 30% prior to deformation when strained at room temperature to 15% elongation (commensurate with passage of the Luders band) all showed a varation in volume percent martensite with distance from the surface. Figures 27a, 27b and 27c show this dependence. Such dependence is present in all the materials examined and seems to be most pronounced in the material with the least prior deformation.

3. Comparison with athermal martensite.

When comparing the general morphology of the strain induced martensite to that obtained by immersion in liquid nitrogen, it is obvious that there are some differences. The strain induced martensite is exemplified in Fig. 23b while the athermal martensite morphology varies, depending on

the amount of PDA. Figures 28a through 28d show the microstructures obtained on quenching 0, 10, 20, and 30% PDA material, respectively, in liquid nitrogen. The strain induced martensite is most nearly like that obtained in some regions of the quenched, undeformed material. Observe Figs. 21 and 28a and 23b for these comparisons. The athermal martensite obtained by quenching the PDA was definitely acicular.

C. Differential Thermal Analysis

It was observed that some martensite was occasionally present in the surface of the initial austenitized material, probably as a result of surface decarburization. This was not detected after the thermomechanical treatment despite the removal of carbon as carbides from the matrix and the consequent raising of the M_s temperature. To understand the reason for this, the austenite start temperature (As) was determined on quenched and strain-induced martensitic structures. The results appeared to be quite independent of the prior treatment or method of obtaining the martensite and the As temperature occurred consistently at 555°±5°C. Figure 29 is one typical differential thermal curve showing the endothermic reaction.

D. Magnetic Measurements

The results of the magnetic saturization determinations of percent martensite are summarized in Fig. 8. It must be noted that no matter the amount of prior deformation the percent martensite was the same in specimens cut at 45° to the rolling direction. The other orientations did not vary directly with amount of prior deformation but showed a minumum in the 20% deformed material. Since these values were measured at failure and not at a constant strain, the comparisons must be made with that in mind.

E. Luders Strain Measurements

Measurement of the relative areas both inside and outside the Luders band on the specimen shown in Fig. 16 showed a relative strain of 10%. In other words, the passage of the Luders band results in a 10% strain over and above that occurring in the material outside the Luders band.

IV. DISCUSSION

The mechanical properties measured in this investigation can be discussed in terms of the thermomechanical treatment and the strain induced martensitic transformations. The deformation during the thermomechanical treatment provides the work hardening necessary to raise the yield strength of the austenite. This process also results in the observed banded microstructure containing relatively large Mo_2C particles. Although the temperature was low enough (500°C) to prevent large rates of diffusion, the concurrent deformation is expected to increase significantly the diffusion rates of the carbon and molybdenum. If the material was originally homogeneous, however, the diffusion rate of molybdenum would still not be sufficient to allow the formation of such large precipitates during the deformation process. It is therefore expected that there existed chemical inhomogeneity prior to deformation so that the diffusion distance of molybdenum need not be so great. Such a condition would result in the observed banded structure.

Evidence of this chemical segregation is demonstrated when the undeformed material is quenched to just below the M_s temperature. Figure 21 shows such a sample which has martensite formed in parallel arrays although there is no evidence of banding precipitates. This indicates modulation of M_s due to chemical inhomogeneity. The austenitizing process, therefore, does not completely homogenize the material and there is retained the chemical segregation originating during casting and aggravated by the forging. The deformation at 500°C merely causes the precipitates to form in regions of high molybdenum content.

No direct evidence of smaller precipitates was observed in the

deformed austenite. Although transmission microscopy shows no conclusive evidence of fine precipitation, optical microscopy of the cross section of rolled sheets show the persistance of slip bands after polishing and re-etching. This lends evidence that the slip planes may possibly be decorated by small precipitates, Fig. 17. Such small precipitates would be very effective in precipitation strengthening. With increased amounts of deformation there is likely to be more precipitation as well as higher dislocation densities; both raise the yield strength.

Transmission electron microscopy of this strain induced martensite exhibits no evidence of twinning as reported by other investigators for similar steels quenched to martensite.[11] Cohen and Taranto[9] propose that the cause for this may be related to the state of the dislocation networks inherited by the martensite. They postulate that the dislocations inherited by the ausformed martensite are not as strongly pinned as would be dislocations arising from martensite which had been strained and then aged. Because of the availability of large numbers of mobile dislocations in the plastically deformed austenite, it is undoubtedly easier for the heterogeneous component of the martensitic transformation shear (the so-called second strain) to take place by slip rather than by twinning.

The 0.1% offset yield points as reported in this paper must be discussed in the light of the strain induced martensitic transformation. Two types of stress-strain curves exist in this material, depending on the treatment. The Luders strain, as will be shown later, is nearly completely due to the transformation strains involved with the martensitic transformation. There is little plastic deformation involved aside from

the transformation strains and, hence, the Luders band front cannot be described as a purely plastic wave front. It is reasonable to expect, in the light of this evidence, that the onset of the Luders strain is merely the beginning of the martensitic transformation and not due to any of the classical mechanisms of yield points. Since there is little plastic deformation (aside from the transformation strains) involved during the Luders strain, it can be said that during the Luders strain the stress required to induce the martensitic transformation is less than the flow stress of the austenite.

In other words, the Luders strain arises when conditions are such that the stress, at a particular low value of plastic strain required to induce the martensitic transformation, is less than the flow stress of the austenite at that same strain.

When the flow stress at a particular strain condition in the austenite is less than or equal to that required to induce the transformation there will be no Luders strain. In this case, plastic deformation of the austenite is concurrent with the strain induced martensitic transformation and no Luders band is formed.

The stress at which the strain induced martensite occurs is increased by increased prior deformation at 500°C as shown by the engineering stress-strain curves. However, the strain required prior to the first martensitic transformation is concurrently reduced by increased prior deformation. A possible explanation for this relates to the combined effect of mechanical stabilization and the opposing increase of M_s as a consequence of precipitation (both C and Mo are removed from the matrix). The mechanical stabilization of the austenite with respect to the

transformation is enhanced with prior deformation as is the yield strength, so the stress required to obtain the strain energy sufficient to cause the onset of the transformation is increased. However, the chemical M_s is raised, at least locally, due to the precipitation. Then, once the stabilizing influences are overcome and the transformation begins due to higher stress, the strain required for the strain induced martensitic reaction is less. This is because the austenite is more unstable with respect to the chemical M_s.

When a certain proportion of martensite is formed in the austenite matrix, the strength becomes such that work hardening begins in a manner similar to that observed in the material not exhibiting the Luders strain. This point delineates the end of the Luders strain.

When the Luders strain was determined by measuring the relative areas both inside and outside the Luders band in a specimen strained to incomplete passage of the Luders band, a 10% strain was observed (Fig. 16). From the Nishiyama relationship[20] for the martensitic transformation in iron-nickel alloys, there is approximately a 19.5° shear angle involved in the crystallography of the transformation. This amounts to a strain of about 35.4%. The microstructural observations of the amount of martensite in specimens strained to the end of the Luders strain (or equivalent strain in case of its absence) show that the Luders band contains about 35 vol.% martensite. This was found by integrating the curves in Figs. 27a through 27c. Then the strain due only to the shear component of the transformation strain is:

$$\frac{.35 \times 35.4\%}{\sqrt{2}} = 8.8\%$$

This assumes that the shear strain is, on the average, oriented at 45°

to the tensile axis. The components perpendicular do not contribute as much to the strain while the components parallel to the tensile axis contribute more. There is also associated with the transformation a 1.4% length change due to the volume dilation.[21] Its contribution is: .35×1.4% = .5%.

Therefore the total strain due solely to the transformation strain is approximately 8.8 + .5 = 9.3%. This agrees quite well with the measured strain.

It can be postulated, with this evidence, that the Luders strains observed in the metastable austenitic alloys of this investigation are due mostly to the martensitic transformation strains. The difference between the strain calculated above and the observed values of 10-15% for the Luders strain must be contributed to the plastic strain of the austenite outside the Luders band and perhaps to some deformation of the austenite as a result of the transformation strains. The surface topography of the austenite outside the Luders band shown in Fig. 16 is ample evidence that some plastic deformation occurs prior to the passage of the Luders band. It is not known if this occurs solely prior to the onset of the Luders strain or is increased during the Luders strain.

The distribution of the martensite as shown in Figs. 27a-27c, where the amount of martensite is greater near the surface of the tensile specimen, is probably due to two effects. The first effect would be due to the biaxial stress conditions at the Luders band front. These conditions are more conducive to the martensitic transformation. The other factor, present even in the absence of a Luders band, is the reduced volume constraint near the surface. The fact that the strain-

induced martensite develops first near or at the surface in the material which had received no prior deformation demonstrates that the presence of a Luders band is not a prerequisite for the type of martensite distribution observed. The effect of decarburization has been eliminated as a possible cause by removal of about .010 in. from the surface prior to testing.

Following the Luders strain (or equivalent total strain for those specimens not exhibiting the Luders strain) there is a portion of the stress-strain curve with a high work hardening rate and work hardening exponent. The second phase, martensite, serves to increase the work hardening rate. The strain induced martensite serves perhaps its most important role in the properties of the metastable austenite in this portion of the curve. Regions subject to higher strain will, of course, tend to have the largest amount of strain induced martensite appearing. When an area of gage section begins to neck, this area is subject to a localized increase in strain. Due to this, an increased amount of martensite is locally induced. The newly formed martensite is inherently stronger than the austenite from which it is formed and as a result the necking is prevented at this point. The above procedure repeats itself until the stress is high enough so that the strength of the two phase material is not high enough to prevent necking even in the presence of the strain induced martensite. This sequence of events is similar to that proposed by Bressanelli and Moskowitz in stainless steels.[15] This limit is probably due to the inherent ultimate strength of the martensite formed.

Further evidence that this process is limited by the strength of the strain induced martensite can be provided by observing that the

ultimate true stress in the 10% deformed sample quenched into liquid nitrogen is approximately 200,000 psi, while the same material without quenching exhibits a true maximum stress of about the same value.

Superimposed on the stress-strain curve, beyond the Luders strain, is a series of serrations consisting of very rapid load drops with subsequent high work hardening rate. The magnitude of these load drops increases at higher strains. These load drops have been associated with the martensitic transformation by Zackay et al.[1] and Chanani.[22] Their explanations involve the transformation strains accompanying the transformation which momentarily reduces the load. Bressanelli and Moskowitz[15] associate these load drops with a local increase in temperature due to the higher strain rate in the necked area. Because of the high strain rate at the neck, martensite forms, preventing further flow. Another explanation presented by this author proposes a mechanism of strain aging, whereby the martensite appearing during straining is subject to the heat of the transformation and the heat due to the plastic deformation. According to Cohen,[23] carbon can diffuse a sufficient distance to have an aging effect in Fe-Ni-C martensite in a matter of seconds or minutes at room temperature. Since the martensite is certainly subject to higher than room temperature, aging is expected to occur. The freshly occurring martensite is not likely stressed beyond its yield point. However, as this aging occurs, with the stress concurrently being increased, the yield strength of the martensite and the stress are approaching each other. The size of the precipitates, as previously mentioned, necessary to cause this aging may be too small to resolve in the electron microscope.

This aged martensite then exhibits yielding when the stress on it reaches the current yielding stress causing a yield drop or serration.

The yielding of these martensite plates can cause very high localized straining in the adjoining austenite causing more martensite to nucleate. Hence, in any of the cases discussed, the serration can be associated with the martensitic transformation.

A test should be performed to decide if the aging effect is important. A tensile test would be run at a sufficiently low temperature but above the M_s and in a circulating fluid bath to minimize the effect of any heating. The absence of any serrations when straining would indicate the possible absence of the aging effect or support conclusions of Bressanelli and Moskowitz.[15] The test would then be stopped below the maximum load and the specimen warmed to room temperature for a period of time then reloaded at the original test temperature. If serrations then appeared, the aging mechanism for the serrations would be said to be a factor. Two Russian investigators[24] report serrations in the stress-strain curve of a hydrogenated nickel alloy while these serrations were absent when no hydrogen was present. They show that the serrations are due to a strain aging effect where some of the dislocations are immobilized by precipitates or solute atmospheres. Brindley and Barnby[25] show stress-strain curves of mild steels undergoing dynamical strain aging which are very similar in appearance to those obtained in TRIP steels with the serrations occurring in the strains following the Luders strain. The possible occurrance of such a mechanism is enhanced in the material under current investigation since the martensite, when first formed, is not being plastically strained and a large number of the dislocations are not moving.

The fact that many, but not all, of the strain induced martensite plates occur at an orientation with respect to the tensile axis equivalent to the necking line of the tensile instability in flat strip tensile specimens leads to the conclusion that two factors may contribute to the morphology of the martensite.

The first factor is the general slip occurring as a result of uniform plastic deformation of the austenite. In this case the martensite plates would most likely form in such a manner as to best relieve the strain energy commensurate with requisite crystallographic relationships. Such a strain induced martensite would, therefore, give a morphology termed "Bracket" martensite by Maksimova and Nikonorova.[26] They report that the criterion governing the arrangement of the strain induced martensite plates is that of maximum relief of the applied stress. This is best achieved when the deformation produced by each martensite plate has at least a large component in the direction of stress. This leads to the production of martensite plates joined in pairs at an obtuse angle.[27] Figures 23b and 23c show many instances where martensite grains are joined at obtuse angles. This may explain, in part, the difference in morphology between the strain induced and the athermal martensites.

The second factor is related to the state of stress accompanying the necking. This highly biaxial stress condition lying at about 54.7° (Ref. 19) to the tensile axis tends to promote the strain induced transformation by reducing the elastic volume constriction which is then added to the increased amount of shear strain present in that region. The martensite so formed

would, of course, tend to form only upon the start of necking and would often lie in planes parallel to the necking line. The orientations are, of course, limited by the necessary crystallographic relationship. Figure 24 shows these plates as they are related to the tensile axis. After the transformation the necking would, at this point, be stopped and it would proceed to an adjacent area explaining the existence of parallel martensite plates shown in Fig. 24.

The combination of these two mechanisms is most often the case and the resulting morphology of the strain induced martensite found in the gage section of a tensile specimen is a mixture of both types of morphology as seen in Figs. 21a and 21b.

A third type of morphology of the strain induced martensite is observed only in the tensile specimens of the material which had been austenitized without receiving the thermochemical treatment. As shown in Fig. 21c, this martensite appears to have no particular orientation relationship with respect to the tensile axis. It does not form in large amounts until late in the tensile test when necking has progressed extensively. The reduced volume constraint appears to be a major factor here and the martensite then forms in the morphology which best relieves the stress condition consistent, of course, with the requisite crystallographic relationships.

The athermal martensite formed by cooling in liquid nitrogen is of much different morphology than that occurring as a result of strain. Figures 25b and 25c show that the martensite formed in the materials with prior thermomechanical treatment then quenched in liquid nitrogen were lenticular in appearance with the "lightening-bolt" relationship between

neighboring plates. These lightening-bolt-like plates become more clearly delineated in the materials that had received some prior deformation at 500°C. Definite midribs are observed in the athermal martensite while none were observed in the strain induced martensite. The reason for these observations is probably due to the temperature of the reaction. The material with prior deformation had been mechanically stabilized, and therefore, transformed at a lower temperature. It should be noticed that when the martensite was formed at a higher temperature (Fig. 21), the appearance of each individual plate, although not its orientation, is very similar to that of the strain induced martensite (Fig. 23b).

The morphology of each plate, then, appears to be a function of the temperature of formation although the tensile mode of deformation tends to cause a preferred type of orientation relationship of the plates as discussed before.

The data on tensile strength, work hardening exponent, work hardening rate and total elongation when measured in tensile specimens cut at 0°, 45° and 90° to the rolling direction all showed nearly the same properties in the 0° and 90° specimens.. The 45° specimens showed increases in tensile strength, work hardening rate and exponent and a decrease in total elongation. The yield strength variation with orientation was negligible.

This variation with orientation can and should be discussed in terms of the amount of martensite occurring during straining. Figure 8 shows how the amount of martensite, at tensile failure, varied with orientation.

This shows that the specimens cut at 45° to the PDA rolling direction all had the highest amount of martensite. As mentioned in the previous discussion, the occurrance of the strain induced martensite is what results in the properties of high tensile strength, and high work hardening rate. The total elongation is limited by the inherent strength of the martensite and the point during the test at which it is nucleated. Figure 10 shows that with increasing prior deformation up to about 20% the tensile elongation reduces, indicating that the strengthening effect prior deformation has on the subsequently formed martensite is more than offset by the fact that the martensite is formed early in the test and reaches a maximum with less strain. Then its potential to prevent necking is exhausted. However, with a further increase in prior deformation at 500°C the austenite becomes more stabilized and the elongation appears to take an upward swing. In this later case, only the higher amounts of strain accompanying necking will induce the transformation.

The question as to why the 45° specimens formed more martensite is easily answered by considering the composition modulations discussed earlier. These modulations are schematically portrayed in Fig. 19 along with schematic portrayals of the gage sections of tensile specimens cut at 0°, 45°, and 90° to the tensile axis. The cross-hatched bands in this figure represent regions where the alloy concentration was high and the subsequent M_s lower than the material in the light bands. The light bands are, therefore, less stable with respect to the martensitic transformation than the dark bands.

It can be seen that by any of the proposed mechanisms of strain induced transformation there would be less restriction to the propagation

of martensite plates considering the chemical stability only. The longer "free path," with respect to maximum shear stress and the necking line are greatest in the 45° specimens and about the same in 0° and 90° specimens. If the properties are due mostly to the martensitic transformation, as postulated in this discussion, then those conditions most favorable to the martensitic transformation would be those most favorable to the high tensile strength and high work hardening rate and other associated properties. This is exactly the situation observed in that the modulations are obviously present as are the directional properties.

Elimination of the chemical modulations would, therefore, minimize the directional properties leaving only the variations due to texturing.

Subsequent to this investigation tests were made to determine the conditions necessary to eliminate the chemical modulation. It was found that a 1250°C austenitization for no less than four hours was required to remove all traces of the chemical modulations present after casting and subsequent forging.

The thermomechanical treatment was conducted at a temperature near A_d so that large amounts of deformation are potentially possible without the possibility of strain inducing martensite and, as a result, much higher strengths may be possible.

V. SUMMARY

1. The Fe-22.6Ni-4.02Mo-.28C alloy, when given a thermomechanical treatment of deformation at or about the A_s temperature, produces a metastable austenite with high strength and excellent properties with respect to the prevention of tensile instability.

2. The properties of high tensile strength and high work hardening rate are closely tied to the strain induced martensitic transformation. When modulations of composition are present in this material, directional properties are observed.

3. The stress-strain curves of this material exhibited a Luders strain, providing there was 20% or more prior deformation during the thermomechanical treatment. Below this amount of deformation no Luders strain was noticed. However, when considering the true stress-strain relationship to be according to $\sigma = K\epsilon^n$ all materials showed a change in slope of the $\log_e\sigma$-$\log_e\epsilon$ curves at strain commensurate with the formation of about 35% martensite. Beyond this strain, the curve is a straight line and the slope is considered the work hardening exponent. The value of work hardening exponents obtained range from .44 to .67.

4. Superimposed upon the work hardening part of the curve are serrations. Three possible mechanisms are suggested:

   a. One is that local heating caused by the high local strain rate associated with local necking results in a load drop. This high strain causes the nucleation of martensite which prevents further necking at that point.

b. Another explanation could be that the transformation strains occurring during the formation of martensite cause an imperceptible strain. It is large enough, though, to cause a load drop. The magnitude of these load drops (for the same transformation strain) would probably be increased after the maximum load where necking has reduced the cross-sectional area.

c. A third mechanism may be one involving strain aging where the load drops are caused by the classical yielding of aged martensite on a local scale.

4. The room temperature strain induced martensite is of a much different morphology than the athermal martensite formed from deformed austenite by quenching in liquid nitrogen. The morphology of the strain induced martensite is however similar to that formed athermally from an annealed austenite. The temperature at which athermal martensite is formed appears to govern the morphology in both the deformed and annealed austenites.

5. Many of the strain induced martensite plates lined up parallel to the necking line of flat plate tensile specimens indicating that at least these plates were nucleated during localized necking. The observation that many such parallel plates existed along the gage section indicate that necking was stopped by the formation of a plate proceeding onto an adjacent area. This process then repeats itself resulting in the retardation of necking and hence the enhancement of elongation is realized.

6. The techniques used in preparing this material were such that a highly inhomogeneous distribution of alloying elements resulted. Subsequent operations aggravated these chemical modulations and during the

final thermomechanical treatment there resulted a highly banded microstructure. As a result of this banded microstructure, the tensile properties showed directional variation with respect to the rolling direction.

VI. RECOMMENDATION FOR FUTURE WORK

1. In order to provide a more complete understanding of the TRIP phenomenon, work should be carried out utilizing single crystals to study the strain induced martensitic transformation and large grain polycrystals to study the processing variably.

2. Homogenization at high temperatures followed by ice brine quench provides a homogeneous material. However, the properties of this material after the subsequent TRIP processing are not the optimum. An investigation of homogenization temperature and the temperature from which the quench is initiated should be carried out with a view to optimizing these parameters.

3. One parameter which must be investigated is that of the temperature loss through the rolls. The rolls are at a lower temperature than the specimen and the heat flow effects are not known but are expected to be considerable in their sections.

ACKNOWLEDGEMENTS

The author wishes to express his grateful appreciation to Professors V. F. Zackay and G. Thomas of the Department of Mineral Technology, University of California, for their encouragement and support throughout the course of this investigation. Thanks also are due to Dr. Dan Merz and Mr. W. W. Gerberich for their many helpful discussions and support.

A special thanks is extended to Gloria Pelatowski of the University of California Department of Mineral Technology for her help in preparing the art work and to Mrs. Pat Shand for her patience and endurance in typing the manuscript.

This work was performed under the auspices of the United States Atomic Energy Commission through the Inorganic Materials Research Division of the Lawrence Radiation Laboratory.

REFERENCES

1. V. Zackay, E. R. Parker, D. Fahr, and R. Busch, Trans. ASM 60, 252 (1967).
2. E. M. H. Lips and H. Van Zuilen, Metals Progress 66, 103 (1954).
3. D. J. Schmatz and V. F. Zackay, Trans. ASM 52, 321 (1960).
4. E. B. Kula and S. L. Lopata, Trans. AIME 215, 980 (1959).
5. R. A. Grange and J. B. Mitchell, Trans. ASM 53, 157 (1961).
6. K. J. Irvine et al., JISI 196, 66 (1960).
7. V. F. Zackay, Y. W. M. Justusson, JISI Special Report 76, 14 (1962).
8. I. Tamura, Iron and Steel Inst. of Japan, Transactions 6 [6], 249 (1966).
9. M. Cohen and J. Taranto, ARL 63-124, July (1963).
10. G. Thomas, D. Schmatz and W. W. Gerberich, High Strength Materials, John Wiley and Sons, Inc., 1965, p. 251.
11. O. Johari and G. Thomas, Trans. ASM 58, 563 (1965).
12. W. Gerberich, C. Martin and L. Raymond, Trans. ASM 57, 324 (1964).
13. W. J. M. Tegart, Elements of Mechanical Metallurgy, MacMillan Book Company, New York, 1966.
14. R. Hiltz, Trans. AIME 215, 138 (1959).
15. J. Bressanelli and A. Moskowitz, Trans. ASM 59, 223 (1966).
16. W. Rostoker and J. R. Dvorak, Interpretation of Metallographic Structure, Academic Press, New York, 1965, p. 198.
17. B. de Miramon, (M.S. Thesis), University of California, Sept. 1967.
18. C. Kittel, Ed., Introduction to Solid State Physics, 3rd Edition, John Wiley and Sons, New York, 1967, p. 470.

19. F. A. McClintock and A. S. Argon, Mechanical Behavior of Materials, Addison-Wesley, Reading, Mass., 1966, p. 321.

20. R. Smoluchowski, J. E. Mayer, and W. A. Weylends, Phase Transformations in Solids, John Wiley and Sons, New York, 1951, p. 631.

21. R. E. Reed-Hill, Physical Metallurgy Principles, Van Nostrand, New York, 1964.

22. G. R. Chanani, M. S. Thesis, University of California, Sept. 1967.

23. M. Cohen, Trans. AIME 224, 638 (1962).

24. Y. P. Neckay and K. V. Popov, Physics of Metals and Metallography, 19, [4], 117 (1965).

25. B. J. Brindley and J. T. Barnby, Acta Met. 14, 1765 (1966).

26. O. P. Maksimova and A. I. Nikonorova, Prob. Metalloved. Fiz. Metal. 4, 123 (1955).

27. P. M. Kelley and J. Nutting, JISI 197, [1], 199, (1961).

FIGURE CAPTIONS

Fig. 1 Room temperature engineering stress-strain curve for material having had prior deformation of 20% by rolling at 500°C. Specimen was cut parallel to the rolling direction.

Fig. 2 Room temperature engineering stress-strain curve for material having had prior deformation of 20% by rolling at 500°C. Specimen was cut from the rolled strip at 45° to the rolling direction.

Fig. 3 Room temperature engineering stress-strain curve for material having had prior deformation of 20% by rolling at 500°C. Specimen was cut perpendicular to the rolling direction.

Fig. 4 Room temperature engineering stress-strain curve for material having had prior deformation of 10% by rolling at 500°C. Specimen was cut parallel to the rolling direction.

Fig. 5 Room temperature engineering stress-strain curve for material having had prior deformation of 30% by rolling at 500°C. Specimen was cut parallel to the rolling direction.

Fig. 6 Room temperature yield strength and tensile strength for various amounts of prior deformation (0, 10, 20, 30%) at 500°C as a function of the specimen orientation with respect to the rolling direction.

Fig. 7 Work hardening exponent "n" for the material with various amounts of deformation at 500°C (0, 10, 20, 30%) as a function of the specimen orientation with respect to the rolling direction.

Fig. 8 Volume % martensite in tensile specimens tested to failure for various amounts of deformation (10, 20, 30%) as a function of

the orientation of the specimen with respect to the rolling direction. Measurements were made by magnetic saturization techniques in the vicinity of the fracture after room temperature tensile test.

Fig. 9 Total elongation in room temperature tensile tests for various amounts of prior deformation at 500°C (0, 10, 20, 30%) as a function of the orientation of the specimen with respect to the rolling direction.

Fig. 10 Total elongation in room temperature tensile tests for specimens cut parallel to the rolling direction and at 45° to the rolling direction as a function of the total amount of prior deformation at 500°C.

Fig. 11 Work hardening exponent "n" for various specimen orientations with respect to the 500°C rolling direction as a function of the amount of prior deformation at 500°C.

Fig. 12 Work hardening rate "$d\sigma/d\epsilon$" in room temperature tensile test for various orientations with respect to the 500°C rolling direction as a function of amount of deformation at 500°C. $d\sigma/d\epsilon$ taken at $\epsilon = .15$.

Fig. 13 Work hardening rate "$d\sigma/d\epsilon$" in temperature tensile test for various orientations with respect to the 500°C rolling direction as a function of amount of deformation at 500°C. $d\sigma/d\epsilon$ taken at $\epsilon = .20$.

Fig. 14 Work hardening rate "$d\sigma/d\epsilon$" in room temperature tensile test for various orientations with respect to the 500°C rolling direction as a function of amount of deformation at 500°C. $d\sigma/d\epsilon$ taken at $\epsilon = .25$.

Fig. 15 a-j log true stress vs. log true strain plots for the stress strain curves obtained in this investigation. Note the straight line sections all occurring beyond about the same strain. It was in these sections that the work hadrening exponent "n" was measured.

Fig. 16 a-d Tensile sample which had been propolished then strained at room temperature 3.5%. The material had received 30% deformation by rolling prior to cutting the tensile sample parallel to the rolling direction. Note the occurrence of considerable plastic deformation outside the "Luders" band and marked surface upheavals inside the "Luders" band. At this stage the area inside the "Luders" band was strongly attracted by a hand magnet while that outside was not.

Fig. 17 Cross section of material after 30% deformation at 500°C in three passes through the rolls. Note the heavily banded microstructure. In some areas, slip bands persisted after repolishing and re-etching indicating that there were some very small-precipitates decorating the slip bands.

Fig. 18 Electron microprobe step trace across some of the banded microstructure of Fig. 17. Mo L_{α} was measured in counts per 10 sec. Similar traces detecting iron and nickel failed to show any significant variations as the trace crossed the heavy bands.

Fig. 18 Schematic protrayal of the material after thermomechanical treatment in which solute concentration is modulated as a result of the incomplete homogenization and the heavy bands of precipitation. These chemical modulations then lead to modulations of M_s temperature across the structure. The three

tensile specimen orientations are portrayed along with the lines of maximum resolved shear stress and the necking line. Note that the necking line and maximum shear stress are approximately parallel to these bands of variation of M_s.

Fig. 20 a) Bright field transmission electron micrograph showing some of the larger precipitates in the bands of the microstructure. b) Dark field micrograph utilizing the two diffraction spots indicated. Note that the two precipitates light up. c) Selected area diffraction pattern containing both of the precipitates which reversed contrast in the dark field. Two HCP diffraction patterns of Mo_2C are superimposed on the FCC matrix. As indexed, both precipitates are of the $\langle 12\bar{3} \rangle_{Mo_2C}$ orientation while the matrix is of a $\langle 110 \rangle_n$ orientation.

Fig. 21 Optical micrograph of austenitized material with no deformation quenched to a temperature just below the M_s. Note how the martensite forms in parallel bands.

Fig. 22 Transmission electron micrographs of the material with various thermomechanical treatments.

a) Austenitized with no deformation at 500°C

b) Austenitized with 10% deformation at 500°C. Note the cellular dislocation substructure

c) Austenitized with 30% deformation at 500°C. Note the almost complete absence of a cellular substructure.

Fig. 23 Micrographs of strain induced martensite.

a) In necked region of the tensile specimen having had no no deformation at 500°C. Testing done at room temperature.

b) In material having had 10% deformation at 500°C and then strained 15% at room temperature.

c) In material having had 20% deformation at 500°C and then strained 15% at room temperature.

Fig. 24 Strain induced martensite as it appears in many areas of the tensile specimens. Note that the parallel arrays of the martensite lineup approximately 55° from the tensile axis. In 24a the small grain in the center of the figure seems to have disrupted the pattern of the strain induced martensite.

Fig. 25 Transmission electron micrographs of strain induced martensite. The material had 20% deformation at 500°C followed by 30% elongation in tension at room temperature. There appears to be no twinning or observable precipitation except the large particles carried over from the banded austenite as shown in Fig. 20.

Fig. 26 The polished tensile specimen strained 5% in tension at room temperature. This material had received no prior deformation at 500°C.

Fig. 27 Variations of amount of martensite with distance from surface of tensile specimens strained 15% at room temperature.

a) Material with 10% deformation at 500°C

b) Material with 20% deformation at 500°C

c) Material with 30% deformation at 500°C

Fig. 28 Microstructures of athermally formed martensite obtained by cooling to -196°C in liquid nitrogen.

a) Material with no prior deformation at 500°C

b) Material with 10% prior deformation at 500°C

c) Material with 30% prior deformation at 500°C

d) Material with 20% prior deformation at 500°C, face of rolled strip

e) Material with 20% prior deformation at 500°C, edge cross section of rolled strip

Fig. 29 Differential thermal curve obtained by heating the martensite steel. The vertical scale is proportional to the difference between the specimen and Ni standard temperatures. The sudden change in slope corresponds to the As temperature where the martensite to austenite endothermic reaction begins, causing the specimen to become relatively cooler.

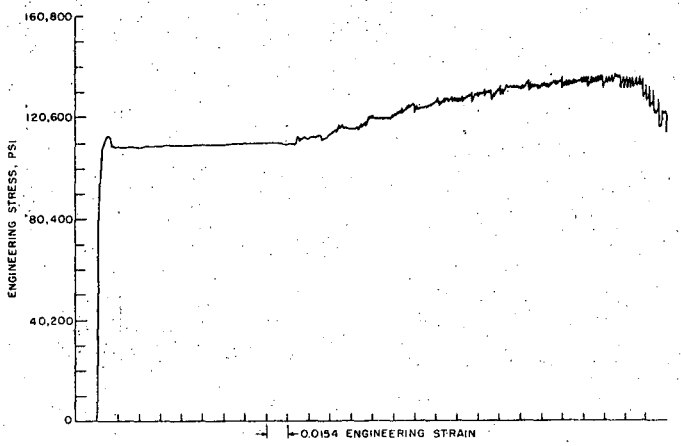

Fig. 1

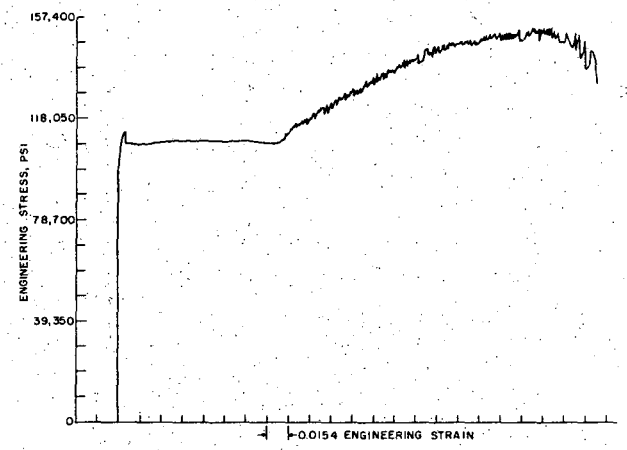

Fig. 2

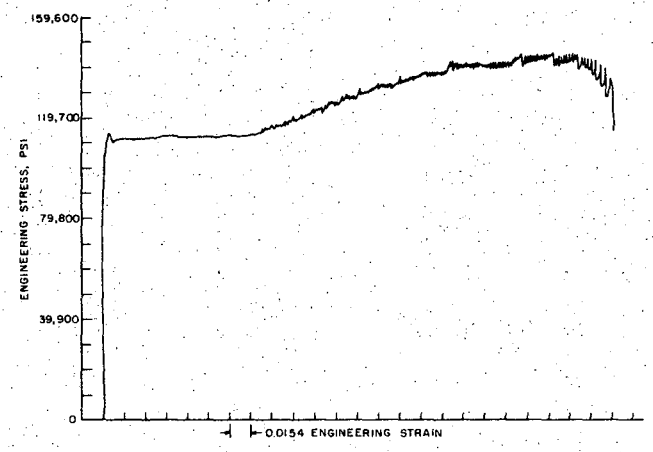

Fig. 3

XBL 685-748

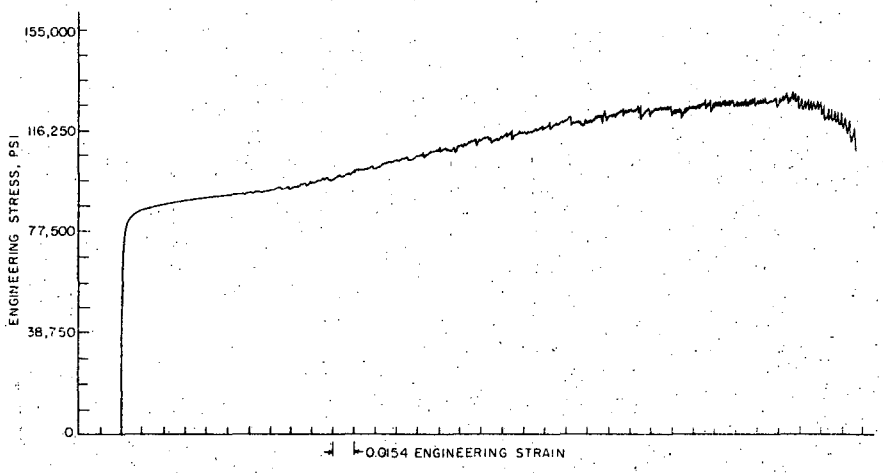

Fig. 4

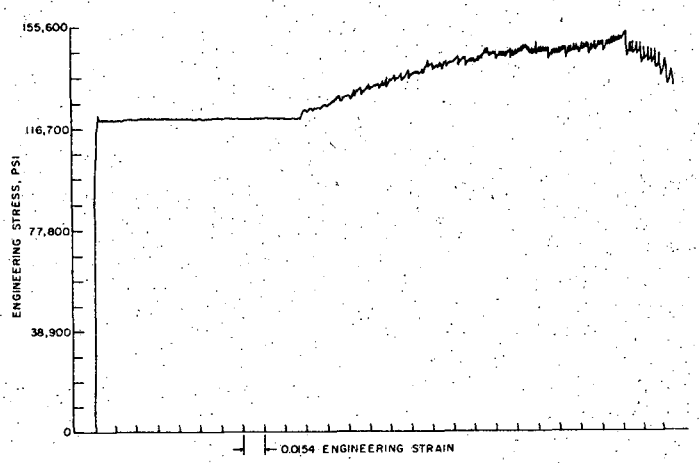

XBL 685-747

Fig. 5

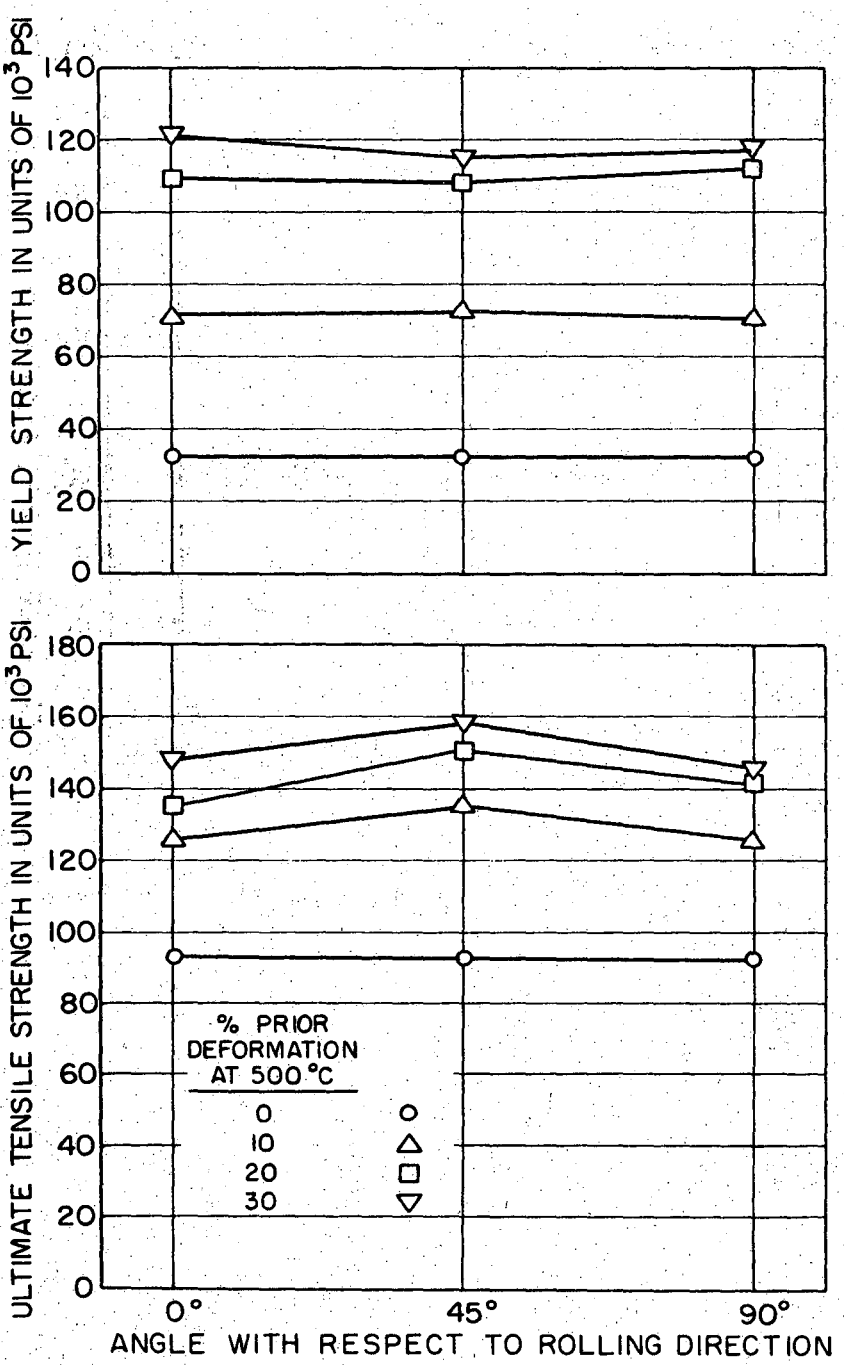
YIELD STRENGTH IN UNITS OF 10^3 PSI
140
120
100
80
60
40
20
0
ULTIMATE TENSILE STRENGTH IN UNITS OF 10^3 PSI
180
160
140
120
100
80
60
40
20
0
% PRIOR DEFORMATION AT 500 °C
0
10
20
30
0°
45°
90°
ANGLE WITH RESPECT TO ROLLING DIRECTION
XBL 685-740

Fig. 6

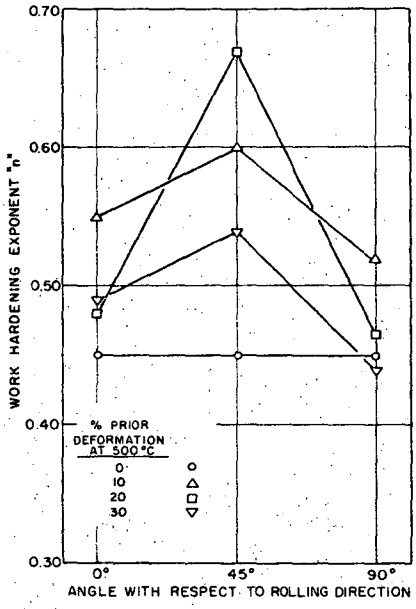

Fig. 7

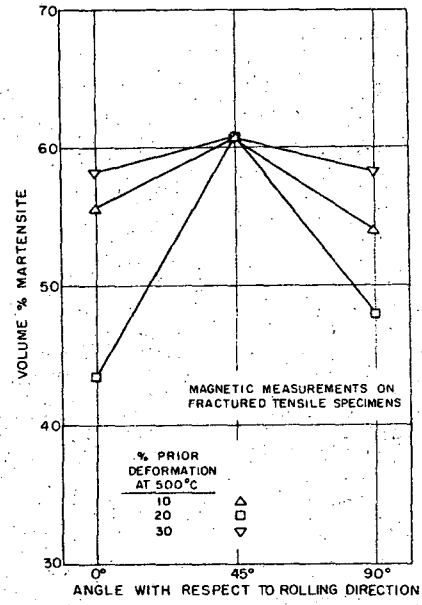

Fig. 8

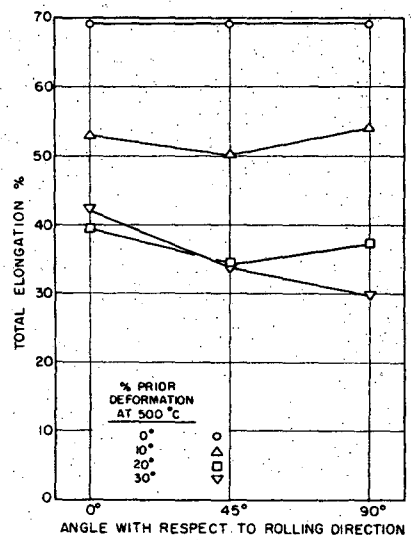

Fig. 9

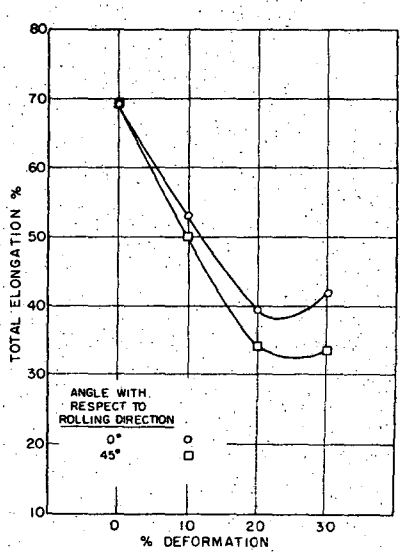

XBL 685-746

Fig. 10

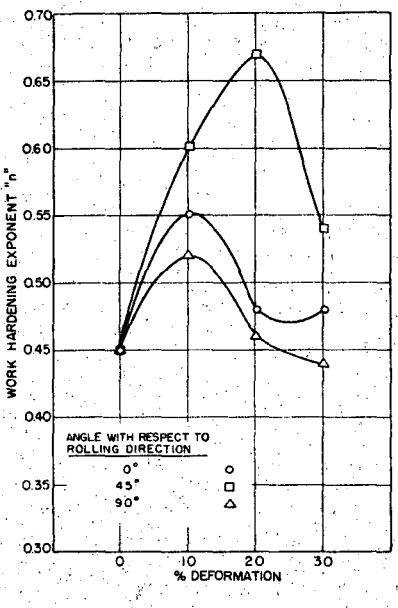

Fig. 11

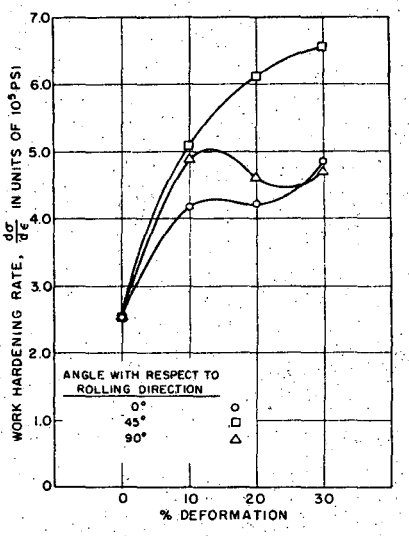

Fig. 12

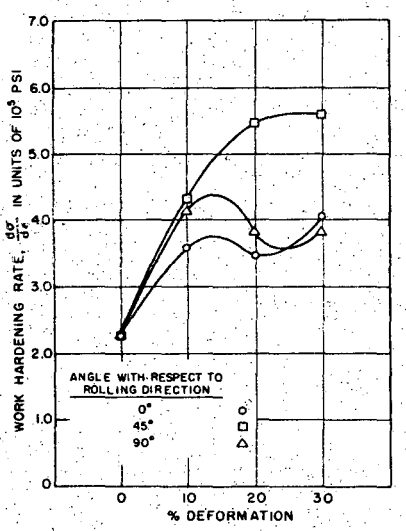

Fig. 13

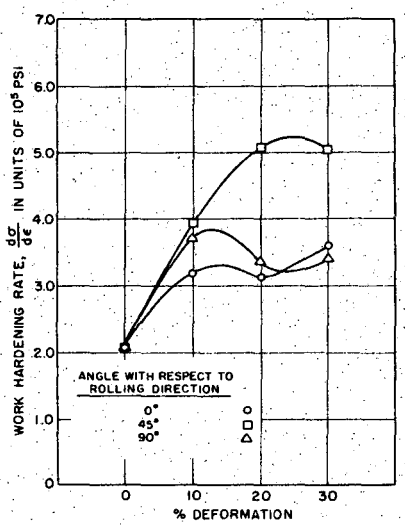

XBL 685-745

Fig. 14

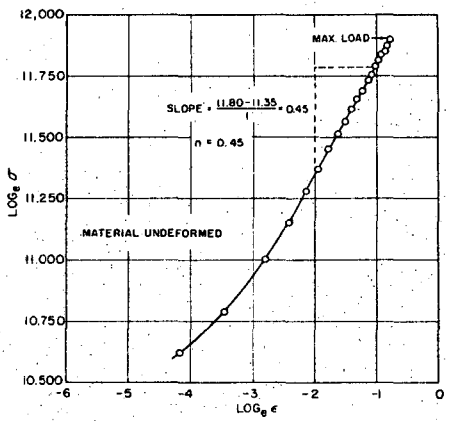

Fig. 15a

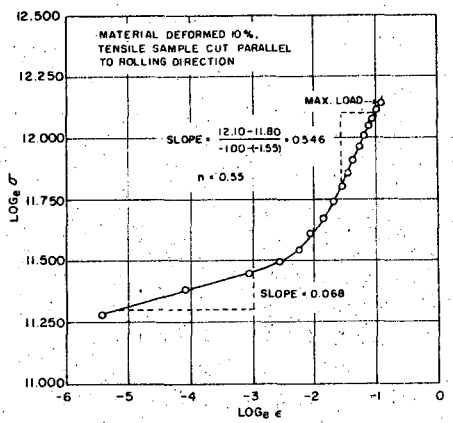

Fig. 15b

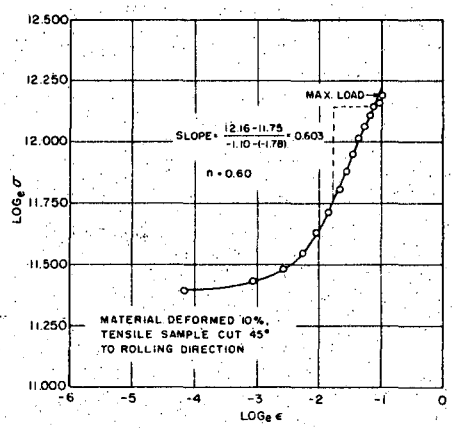

Fig. 15c

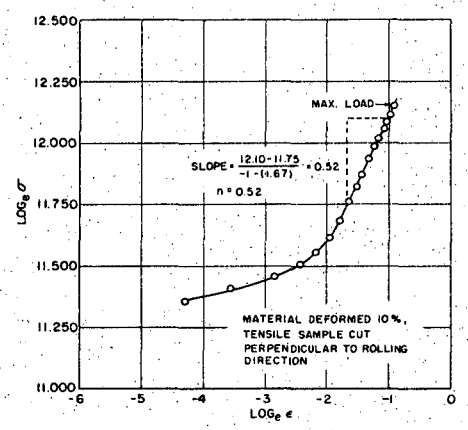

Fig. 15d

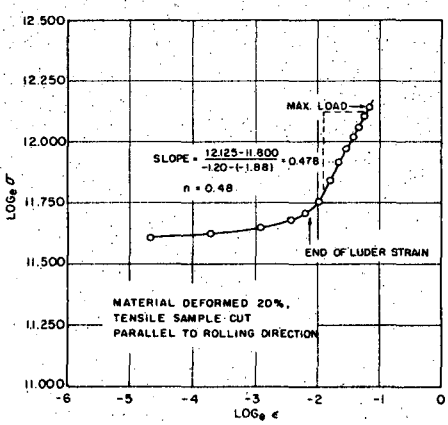

Fig. 15e

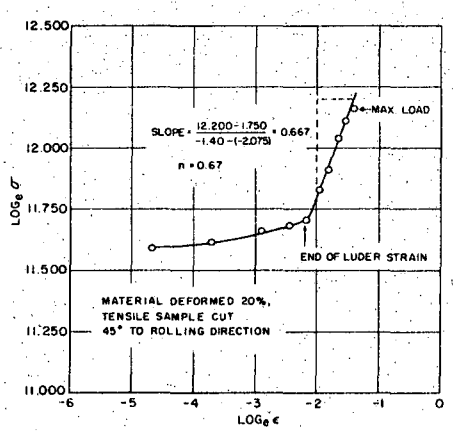

XBL 685-742

Fig. 15f

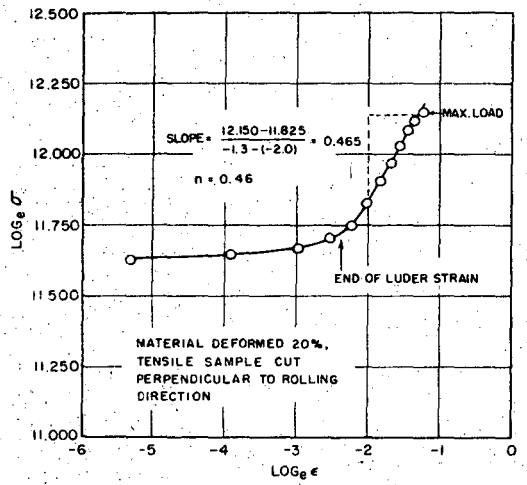

Fig. 15g

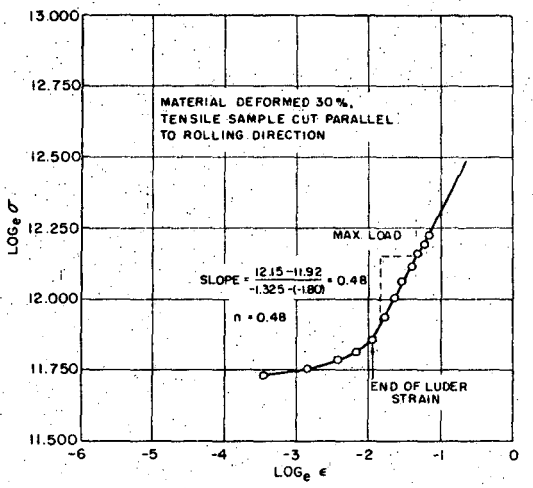

Fig. 15h

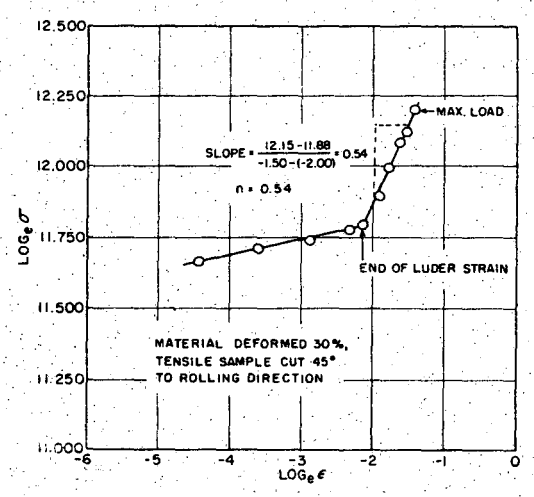

Fig. 15i

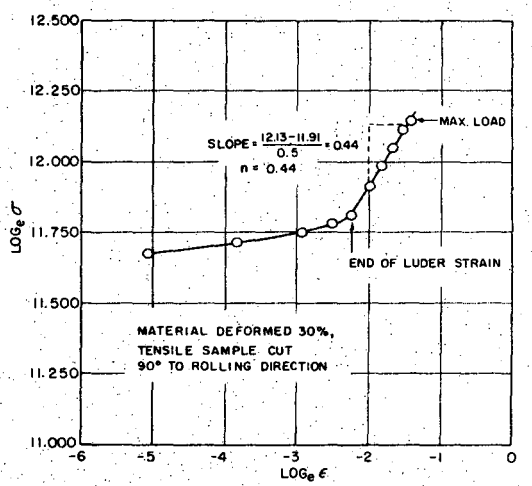

Fig. 15j

XBL 685-743

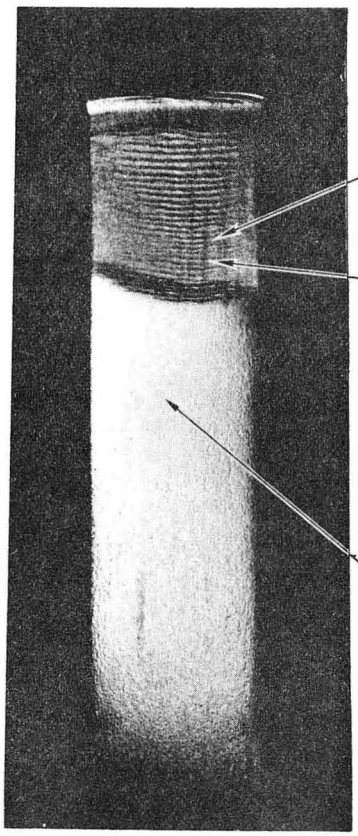

Fig. 16a

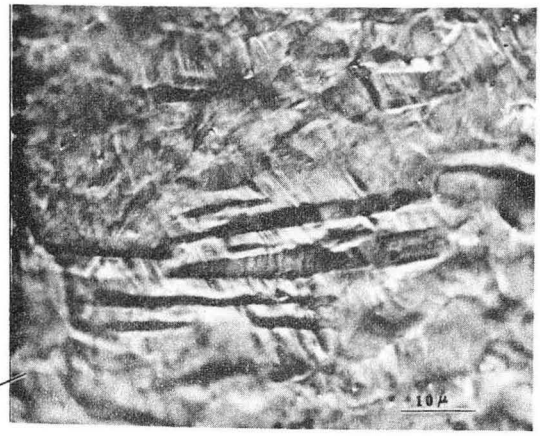

Fig. 16b

Fig. 16c

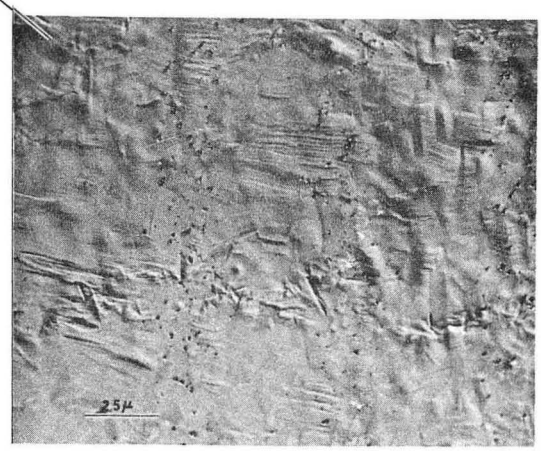

Fig. 16d

XBB 685-2820

XBB 685-2814

Fig. 17

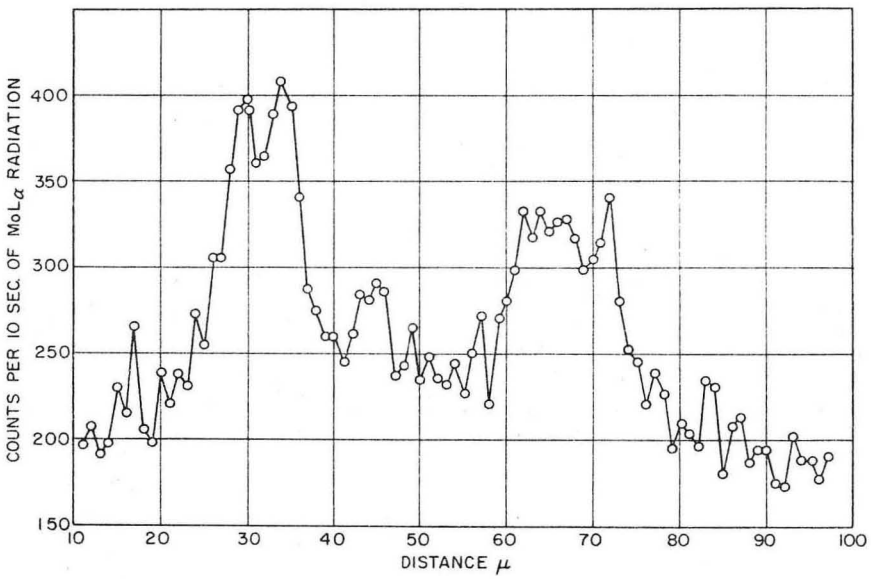

Fig. 18

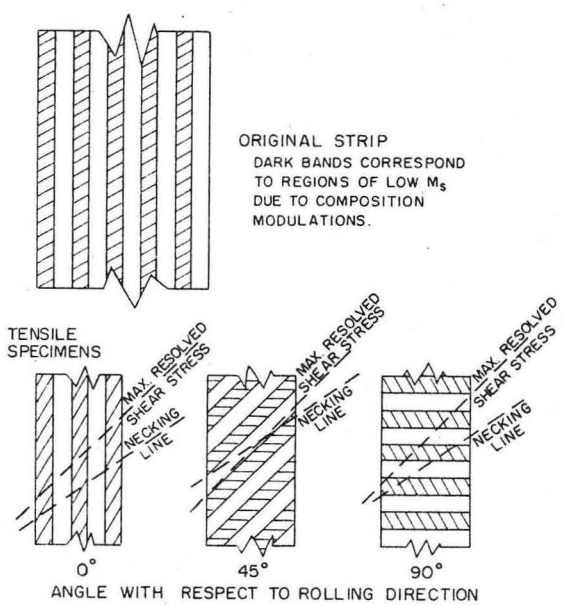

XBL 685-741

Fig. 19

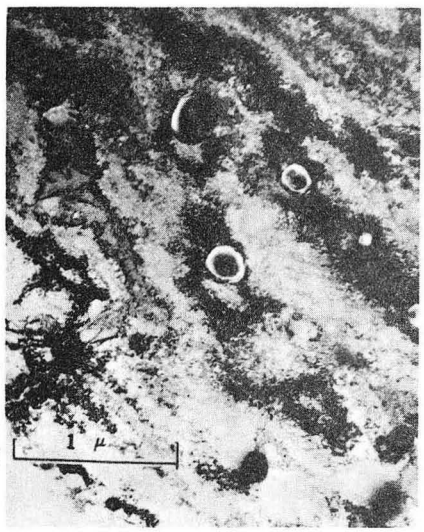

Fig. 20a

Fig. 20b

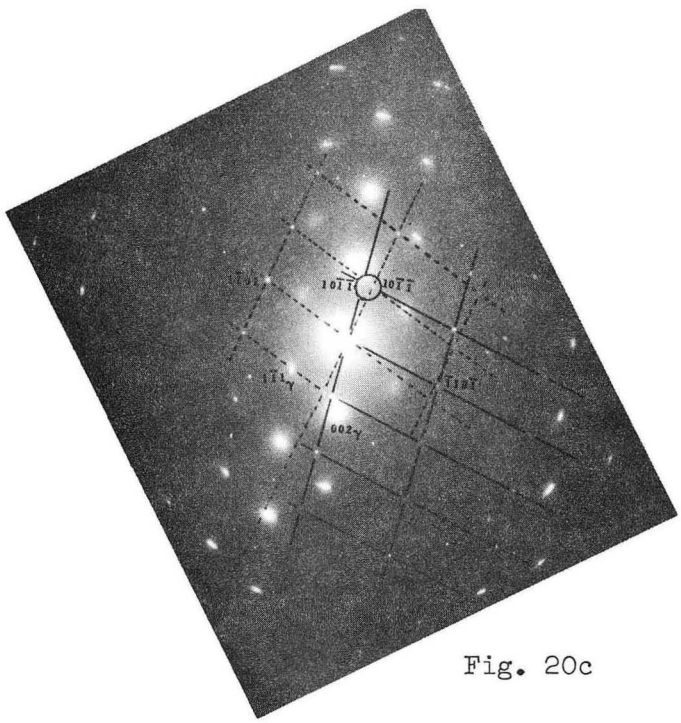

Fig. 20c

XBB 685-2816

XBB 685-2813

Fig. 21

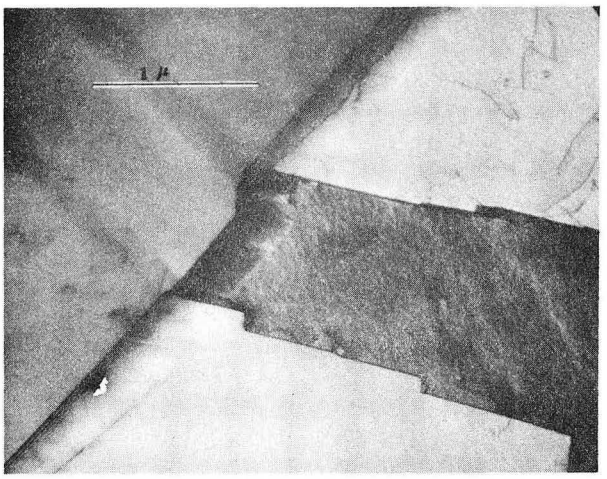

Fig. 22a

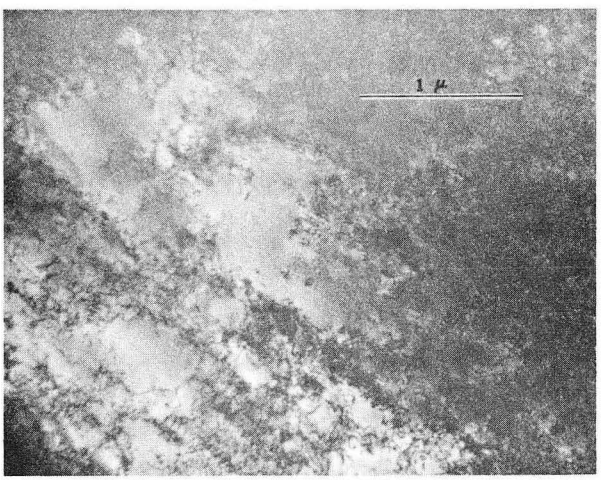

Fig. 22b

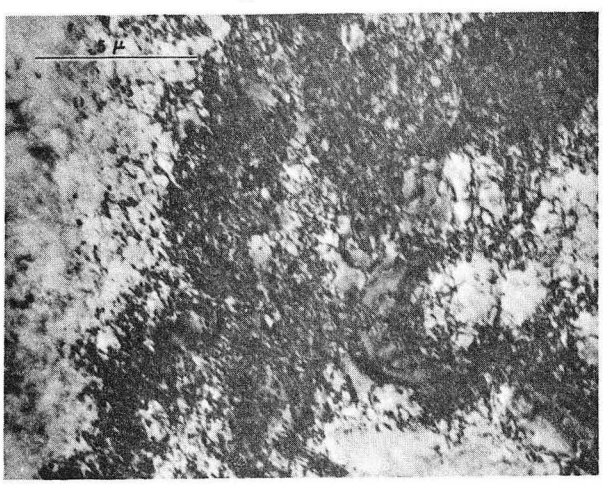

Fig. 22c

XBB 685-2819

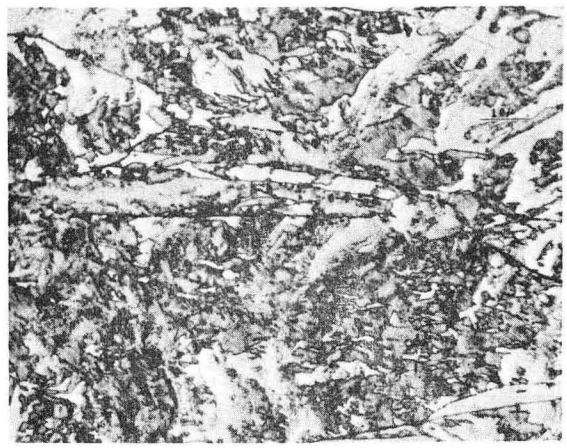

Fig. 23a

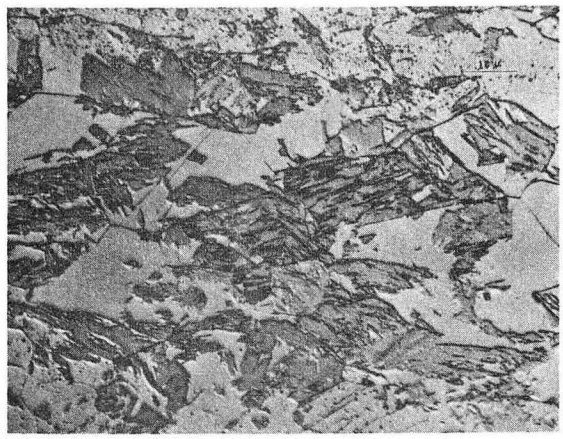

Fig. 23b

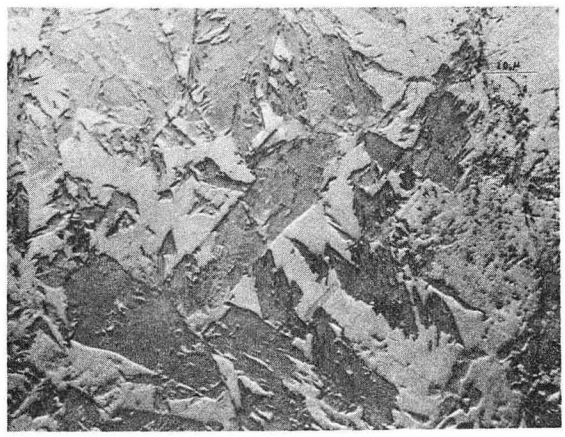

Fig. 23c

XBB 685-2815

Fig. 24a

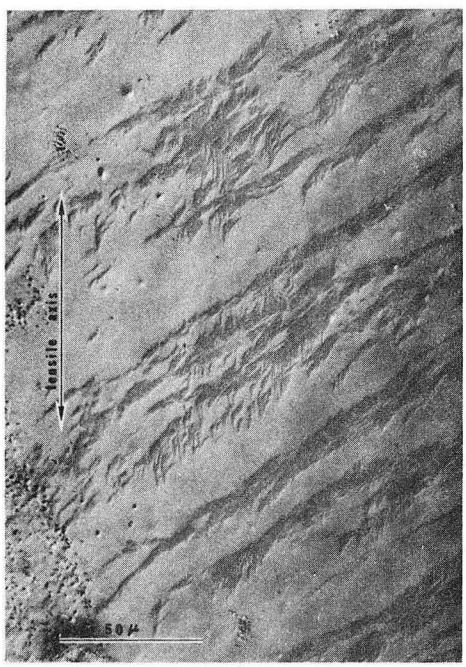

Fig. 24b

XBB 685-2811

XBB 685-2817

XBB 685-2812

Fig. 26

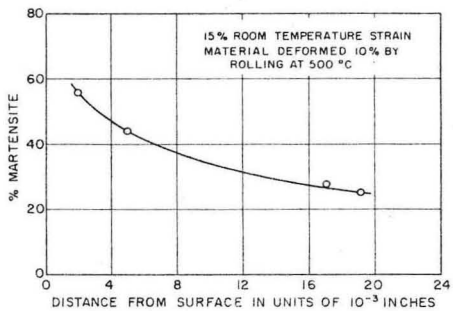

Fig. 27a

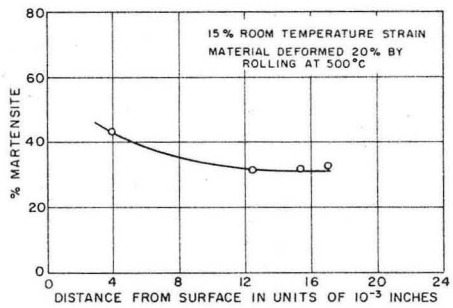

Fig. 27b

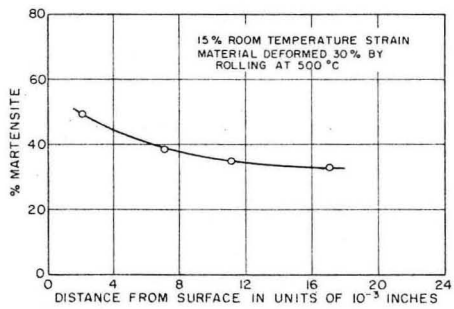

XBL 685-744

Fig. 27c

Fig. 28a

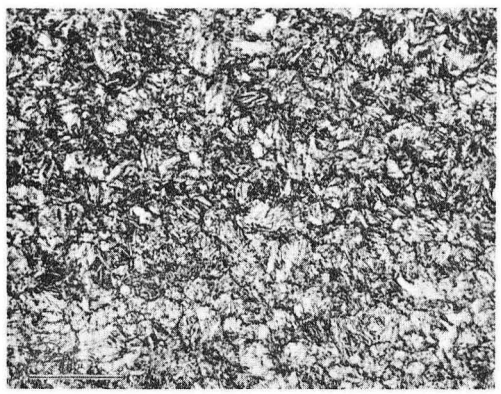

Fig. 28b

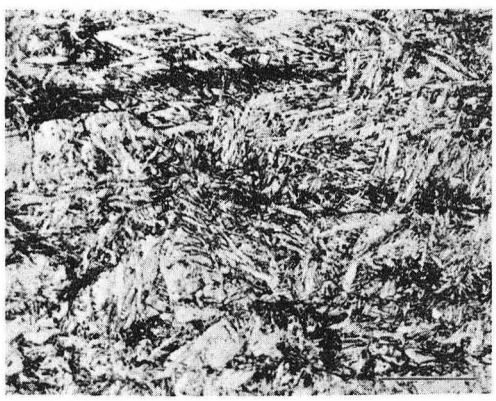

Fig. 28c

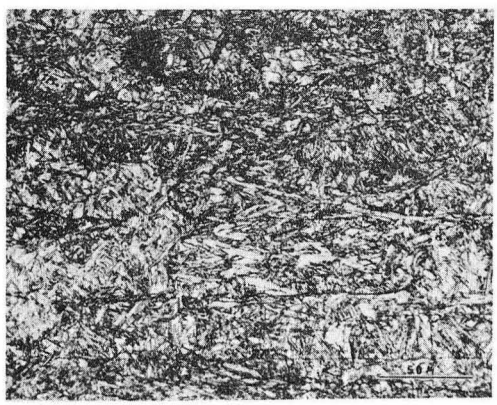

Fig. 28d

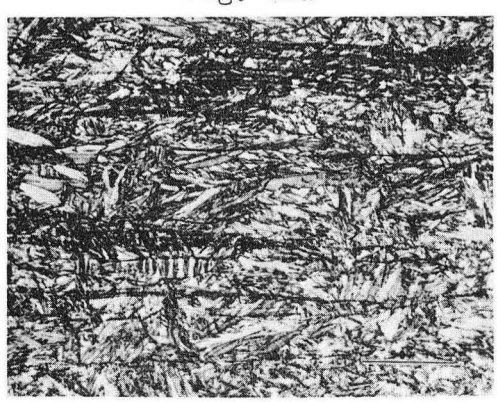

Fig. 28e

XBB 685-2818

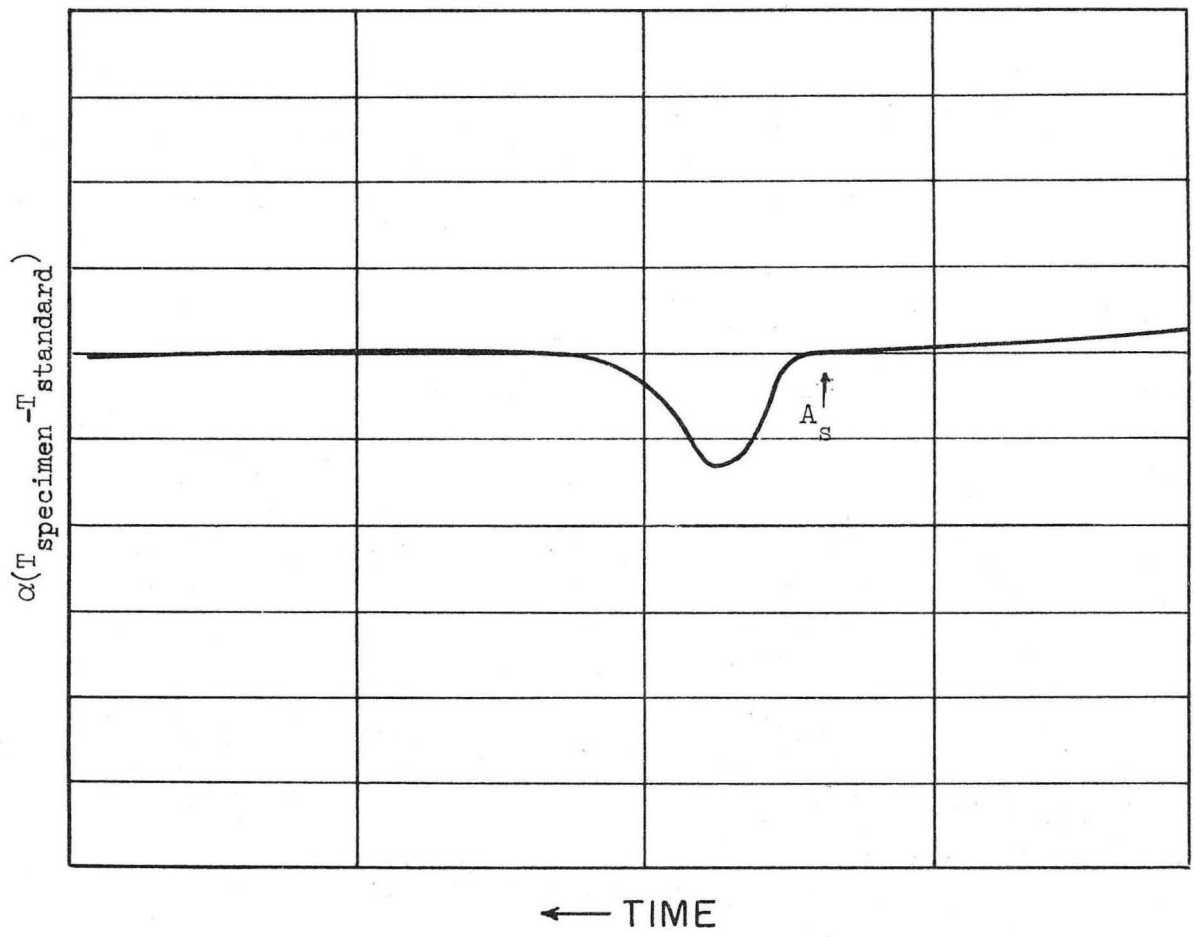

Fig. 29

XBL 685-739